processes

MDPI

*Article*

# Molecular Catalysis of $CO_2$ Reduction with a Zn (II)–Bipyridine Complex

**Gilberto Rocha-Ortiz [1], Brenda Magali Lara-Molinero [1], Luis Gabriel Talavera-Contreras [1], Fernando Cortés-Guzmán [2], Juan Pablo F. Rebolledo-Chávez [3], Gabriela Hernández-Padilla [1], Lillian G. Ramírez-Palma [3], Marisela Cruz-Ramírez [4] and Luis Ortiz-Frade [1,*]**

[1] Departamento de Electroquímica, Centro de Investigación y Desarrollo Tecnológico en Electroquímica S.C. Parque Tecnológico Querétaro, Sanfandila, Pedro de Escobedo 76703, Querétaro, Mexico
[2] Facultad de Química, Universidad Nacional Autónoma de México, Ciudad de México 04510, Mexico
[3] División de Química y Energías Renovables, Universidad Tecnológica de San Juan del Río, Avenida La Palma No. 125 Vista Hermosa, San Juan del Río 76800, Querétaro, Mexico
[4] Colegio de Bachilleres, Universidad Autónoma de Querétaro, Campus San Juan del Río, Calle Corregidora No. 4, Colonia Centro, San Juan del Rio 76800, Querétaro, Mexico
* Correspondence: lortiz@cideteq.mx or laofrade@gmail.com; Tel.: +52-442-2-11-60-65

## Abstract

This work investigates the coordination compound $[Zn(2,2\text{-bpy})_3](BF_4)_2$ as a catalyst for the molecular reduction of $CO_2$. The synthesis and characterization of the complex are reported, along with electrochemical studies conducted both in the presence and absence of $CO_2$. In the absence of $CO_2$, reduction of the 2,2′-bipyridine ligands was observed (Epa(I) = −1.84 V vs. $Fc/Fc^+$ and Epa(II) = −2.18 V vs. $Fc/Fc^+$). In contrast, under a $CO_2$ atmosphere, catalytic molecular activity toward $CO_2$ reduction was detected (Epk(I) = −1.90 V vs. $Fc/Fc^+$ and Epk(II) = −2.18 V vs. $Fc/Fc^+$). Foot of the wave analysis (FOWA) was employed to determine the catalytic rate constant ($k = 1.352 \times 10^3$ $M^{-1}$ $s^{-1}$) for $CO_2$ reduction. Spectroelectrochemical experiments were also carried out in both the presence and absence of $CO_2$. Density functional theory (DFT) calculations were conducted to understand the interaction of the complex with $CO_2$. Bulk electrolysis and FTIR analysis suggest that oxalate is the product of the $CO_2$ reduction.

**Keywords:** molecular catalysis; $CO_2$ reduction; Zn (II)–bipyridine complex; coordination compounds; DFT

check for updates

Academic Editor: Christos Argirusis

Received: 28 September 2025
Revised: 22 October 2025
Accepted: 22 October 2025
Published: 27 October 2025

**Citation:** Rocha-Ortiz, G.; Lara-Molinero, B.M.; Talavera-Contreras, L.G.; Cortés-Guzmán, F.; Rebolledo-Chávez, J.P.F.; Hernández-Padilla, G.; Ramírez-Palma, L.G.; Cruz-Ramírez, M.; Ortiz-Frade, L. Molecular Catalysis of $CO_2$ Reduction with a Zn (II)–Bipyridine Complex. *Processes* **2025**, *13*, 3443. https://doi.org/10.3390/pr13113443

**Copyright:** © 2025 by the authors. Licensee MDPI, Basel, Switzerland. This article is an open access article distributed under the terms and conditions of the Creative Commons Attribution (CC BY) license (https://creativecommons.org/licenses/by/4.0/).

## 1. Introduction

Since the 1970s, global surface temperatures have risen more than during the previous two centuries. Recent years have been the warmest on record, with global temperatures reaching 1.5 °C above pre-industrial levels in 2024 [1,2]. This trend is closely linked to climate change and the intensification of the greenhouse effect. Global greenhouse gas emissions have reached a record high of 53.0 Gt $CO_2$-equivalent, with $CO_2$ as the primary contributor, accounting for 73.7% of total emissions, an increase of 72.1% since 1990 [3]. These figures underscore the unprecedented levels of $CO_2$ emissions resulting from industrial activity.

To address this global challenge, a range of strategies has been developed, from reducing $CO_2$ emissions to capturing and repurposing it. International policies, such as the Paris Agreement, aim to limit emissions, while chemical and physical methods for $CO_2$

capture and utilization have been extensively explored. Technologies such as ammonia-based absorption, low-temperature capture, and adsorption methods have been developed; however, many of these approaches suffer from high energy requirements and efficiency losses, highlighting the need for alternative solutions [4,5].

Beyond conventional fixation strategies, recent research has increasingly focused on converting $CO_2$ into value-added products, particularly liquid fuels that serve as feedstocks for other industrial processes. Among these emerging approaches, the use of coordination compounds for atmospheric $CO_2$ conversion has attracted considerable interest due to their high efficiency and potential scalability.

$CO_2$ is the fully oxidized form of carbon, and its activation remains a major challenge because of its chemical stability, reflected in a large HOMO–LUMO gap (13.7 eV) and low electron affinity [6–8]. Despite its inertness, $CO_2$ exhibits amphoteric behavior: the oxygen atoms can act as Lewis bases and interact with electrophiles, while the carbon atom is susceptible to nucleophilic attack [7]. Breaking the C=O bond requires a substantial energy input of approximately 750 kJ $mol^{-1}$. Given its abundance and environmental impact, $CO_2$ reduction represents a promising pathway to convert it into useful chemical products or fuels.

$CO_2$ reduction involves multi-electron and multi-proton transfer reactions, often leading to a range of products depending on the reaction conditions. Oxalic acid ($H_2C_2O_4$) and formic acid ($H_2CO_2$) are among the primary reduction products, but other species as carbon monoxide (CO), formaldehyde ($CH_2O$), methanol ($CH_3OH$), methane ($CH_4$), and ethanol ($C_2H_6O$) can also be generated [9–12].

Coupling $CO_2$ reduction with chemical processes such as protonation introduces significant complexity [9,11,13,14]. Nevertheless, electrochemical approaches using metal or semiconductor electrodes can directly reduce $CO_2$ by one electron to form the radical anion ($CO_2^{\bullet-}$). A major limitation of this route is the high overpotential required: for example, in aqueous media, a reduction potential of −1.90 V vs. SHE is needed, while in an aprotic solvent such DMF, the potential drops slightly to −1.97 V vs. SHE [9,11,15].

According to electrocatalysis principles, various transition metal-based catalysts can act as redox mediators, facilitating $CO_2$ reduction and helping to overcome the high energy barrier [9,11,15–17]. Over the past three decades, numerous studies have shown that mercury drop and mercury electrodes are highly effective for $CO_2$ electrocatalysis via "sphere-external" mechanisms. However, the toxicity of mercury severely limits its practical applications [15,17].

An alternative strategy for catalyzing $CO_2$ reduction is molecular catalysis, which employs molecular catalysts as electron-transfer agents. An effective molecular catalyst should exhibit rapid electron transfer and thermodynamic compatibility between its redox potential ($E^\circ$) and that of the target reaction. Coordination compounds with tunable steric and electronic properties can be designed to optimize these parameters and enhance the catalytic performance [9,10,17].

In molecular catalysis involving transition metal coordination compounds, several mechanistic pathways have been proposed; however, they commonly involve the coordination of $CO_2$ to the reduced metal center in an inner sphere mechanism. This interaction forms a σ-bond between the metal and the electrophilic carbon atom, generating a species of $M^{n+}L(CO_2)$. The specific coordination mode, degree of protonation ($H^+$ involvement), and number of electron transfers vary depending on the nature of the metal center. For instance, in the reduction of $CO_2$ to CO using a $Co^I(L^{\bullet-})$ complex, $CO_2$ coordinates to form $Co^{II}L(CO_2)$, which undergoes protonation and subsequently releases CO and $H_2O$. In contrast, with an $Fe^I(L)^-$ complex, $CO_2$ coordination results in the formation of an $Fe^{II}L(CO_2)$ intermediate, which undergoes further protonation and electron transfer steps

to produce $H_2CO_2$ as the final product [18]. The acidity of the reaction medium also plays a crucial role in determining the product selectivity among CO, $H_2CO_2$, and $H_2$ [16].

For transition metal coordination compounds to serve efficiently in $CO_2$ molecular catalysis, the catalyst must remain stable throughout both the preparation and reaction processes. Moreover, the catalytic system must include one or more vacant coordination sites to effectively bind and activate $CO_2$, facilitating its reduction [11].

A wide range of macrocyclic ligands, including pyridines, phosphines, and porphyrins, have been incorporated into transition metal complex-based molecular catalysts. Porphyrin-based systems have demonstrated notable efficiency in converting $CO_2$ to CO in the presence of Lewis acids. For example, Fe porphyrins functionalized with N,N-di(2-picolyl)-ethylenediamine (DPEN) exhibit enhanced catalytic activity in acetonitrile, using water as the proton source [19]. Furthermore, introducing Ir or Pd centers in water–acetonitrile mixtures has achieved faradaic efficiencies (FE) of up to 90% [16].

Complexes of Ni, Fe, and Co coordinated with azamacrocyclic ligands have also shown excellent activity for both electrochemical and photoelectrochemical $CO_2$ reduction in organic and aqueous media, yielding $HCOO^-$ and CO with faradaic efficiencies up to 90% [20]. Expanding the range of these ligands and incorporating other metal centers—such as Re, Ru, Ir, Rh, Pd, Os, and Mn—enables the selective conversion of $C_2O_4^{2-}$, CO, or $H_2CO_2$, depending on the reaction conditions [21].

To explore the effects of steric and electronic influences on $CO_2$ reduction, phosphorus-based transition metal complexes, particularly those of Rh, Pd, and Fe, have been investigated. These studies reveal that the redox potential and basicity of the catalyst are key parameters that govern the product selectivity toward $H_2$, $HCOO^-$, or CO. For instance, the Fe complex of tetradentate tris-[2-(diphenylphosphino)-ethyl]-phosphine ($PP_3$), $[Fe(PP_3)(MeCN)_2](BF_4)_2$, has demonstrated excellent electrocatalytic activity for the reduction of $CO_2$ to produce formate ($HCOO^-$), achieving a faradaic efficiency of nearly 97.3% in acetonitrile [22].

Transition metal complexes bearing polypyridine ligands have also been explored for $CO_2$ reduction, demonstrating high catalytic efficiencies and diverse product outcomes [23]. These systems leverage the $\pi^*$ orbitals of polypyridine ligands to store electrons and stabilize the metal center across multiple oxidation states. Molecular catalysts based on Re, Ru, Rh, and Os polypyridine complexes predominantly generate $HCOO^-$, a pathway first reported in 1984 [17]. Additionally, studies using Co(II), Ni(II), Fe(II), and Cu(II) complexes coordinated with 1,10-phenanthroline (phen) or 2-2′-bypiridine (bpy) have shown that product selectivity—favoring CO, $H_2CO_2$, or $CH_4$—depends strongly on the metal center and specific reaction conditions. Table 1 presents examples of compounds that have demonstrated $CO_2$ reduction activity [24–28].

Recent studies have demonstrated the catalytic potential of ZnO in the electrochemical catalysis of $CO_2$ within protic media. It has been reported that ZnO nanorods containing oxygen vacancies, subjected to heat treatment at 500 °C, have exhibited a faradaic efficiency of up to 98% for CO production [29]. Additionally, the heterostructure Cu/ZnO catalyst achieved a 94% faradaic efficiency for CO at an applied potential of −1.3 V vs. RHE. Another variant of Cu/ZnO has been reported to produce $CH_4$ with a faradaic efficiency of 72.4% at a potential of −0.7 V vs. RHE [30–32]. Finally, Zn-based layered double hydroxides (Zn-$M^{3+}$) have been used for $CO_2$ electrochemical reduction to produce CO. The reported results include Zn-Al reaching a 90% faradaic efficiency at −0.96 V vs. RHE, Zn-Cr achieving 92% at the same potential, and Zn-Ga attaining 90% at −0.86 V vs. RHE [33]. These results confirm that Zn metal, in the form of Zn hydroxide or oxide, is a good candidate for $CO_2$ electrochemical catalysis in protic media.

**Table 1.** Examples of first-row transition coordination compounds that have shown evidence of reducing $CO_2$.

| Compound | Applied Potential (V) | Products Obtained |
|---|---|---|
| $[Mn(bipy)(CO)_3Br]^+$ | −1.789 | CO |
| $[Mn(4,4'\text{-dmbpy})(CO)_3Br]^+$ | −1.789 | CO |
| $[Mn(4,4'\text{-dbubpy})(CO)_3Br]^+$ | −2.58 | CO |
| $[Mn(4,4'\text{-dCNbpy})(CO)_3Br]^+$ | −2.2 | $CO + H_2$ |
| [Fe(dophen)(Cl)] | −2.0 | $CO + C_2O_4^{2-} + HCOOH + H_2$. |
| $[Fe(dophen)(N\text{-Melm})_2]^+$ | −2.0 | $CO + C_2O_4^{2-} + HCOOH + H_2$. |
| $[Co(4\text{-mephen})]^{2+}$ | −1.39 | $CO + HCOO^-$ |
| $[Co(4,7\text{-dmphen})]^{2+}$ | −1.39 | $CO + HCOO^-$ |
| $[Co(bpy)_3]^{2+}$ | −1.96 | $C_2O_4^{2-}$ |
| $[Co(tpy)_2]^{2+}$ | −2.28 | $C_2O_4^{2-}$ |
| $[Co(4\text{-PhClphen})_3]^{2+}$ | −3.00 | $CO + H_2$ |
| $[Co(4\text{-PhCH}_3\text{phen})_3]^{2+}$ | −3.00 | $CO + H_2$ |
| $[Co(4\text{-OMephen})_3]^{2+}$ | −3.00 | $CO + H_2$ |
| $[Ni(bpy)_3]^{2+}$ | −1.63 | $CO + CO_3^{2-}$ |
| $[Ni(phen)_3]^{2+}$ | Not specified | $CH_4 + CO$ |
| $[Ni(tpy)_2]^{2+}$ | −1.72 | $CO + H_2$ |

On the other hand, complexes of Zn with polypyridine ligands, such as zinc-bearing tetradentate aminopyridine (N4), Zn−porphyrin complex, or $[Zn(cztpy)_2]^{2+}$ and $[Zn(tpy)_2]^{2+}$ have been reported for photocatalytic $CO_2$ reduction, where both the ligand and the metal center participate in the photoreduction process [34–38]. However, this photocatalytic activity depends on the presence of a photosensitizer [36]. Additionally, another study demonstrated the use of water-stable zinc (II) complexes of neutral pincer bis(diphenylphosphino)-2,6-di(amino)pyridine ("PN3P") for the electrocatalytic reduction of $CO_2$ [36]. These Zn (II) complexes, capable of adopting a range of coordination numbers and geometries, may offer diverse binding sites for $CO_2$ activation.

Such findings can be further investigated using electrochemical methods, particularly cyclic voltammetry, which has been widely employed to study the electrochemical behavior of $CO_2$ reduction [39]. The catalytic response, evidenced by an increase in current at more negative potentials, indicates effective electron transfer between the complex and $CO_2$.

Despite extensive research on Zn-based compounds as catalysts for electrochemical $CO_2$ reduction, Zn (II) complexes with 2-2′-bipirydine ligands remain poorly explored. Therefore, this work presents an electrochemical study of Zn(II) complexes coordinated with the 2,2′-bipyridine in an octahedral geometry, demonstrating their potential as catalysts for $CO_2$ reduction. To evaluate this capability, the catalytic rate constant of $[Zn(2,2\text{-bpy})_3]^{2+}$ was determined. Moreover, spectroelectrochemical experiments were conducted both in the presence and absence of $CO_2$. Possible products were identified by bulk electrolysis and FTIR, and DFT calculations were performed to elucidate the interaction between the reduced complex and $CO_2$. These results provide new mechanistic insights that may contribute to the design of scalable catalytic systems for the conversion of $CO_2$ into high-value products.

## 2. Materials and Methods

### *2.1. Reagents*

2,2′-Bipyridine (Sigma), zinc(II) tetrafluoroborate hexahydrate Stream Chemicals (Newburyport, MA, USA), tetrabutylammonium hexafluorophosphate Sigma-Aldrich, (St. Louis, MO, USA), ethyl ether J.T. Baker, (Radnor, PA, USA), anhydrous ethanol J.T. Baker, (Radnor, PA, USA), anhydrous methanol J.T. Baker (Radnor, PA, USA), potassium bromide Sigma-Aldrich, spectroscopic grade (St. Louis, MO, USA, potassium chloride solution Cole-Parmer, Vernon Hills, IL, USA, dimethyl sulfoxide DMSO, Acros Organics (Geel, Belgium), 99.7% anhydrous, stored over molecular sieves), distilled water, and alumina Buehler (Reno County, KS, USA) were used as received.

### *2.2. Synthesis of [Zn(2,2-bpy)$_3$](BF$_4$)$_2$*

First, 0.3298 g of $[Zn(H_2O)_6](BF_4)_2$ was dissolved in 10 mL of ethanol. Separately, a ligand solution was prepared by dissolving 0.4686 g of 2,2′-bipyridine in 7 mL of methanol. The ligand solution was added dropwise to the zinc solution under constant stirring, resulting in immediate complexation. The mixture was left undisturbed until the solvent evaporated, yielding a precipitate. The product (Figure 1) was then filtered and washed with a mixture of ethyl ether and methanol.

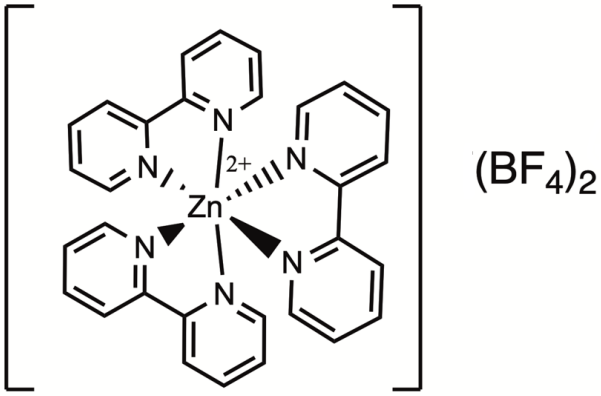



**Figure 1.** Chemical structure of $[Zn(2,2'\text{-bpy})_3](BF_4)_2$.

### *2.3. Characterization of the Coordination Compound*

Conductivity measurements were performed using a Corning Pinnacle 542 pH/conductance (New York, NY, USA) meter equipped with a Corning M542 parallel plate electrode (cell constant = 1 $cm^{-1}$). A standard 1 mM potassium chloride (KCl) solution in DMSO (Cole-Parmer) was used as the reference. The specific conductivity ($\kappa$, S $cm^{-1}$) was determined, and the molar conductivity ($\Lambda$, S $cm^2$ $mol^{-1}$) was subsequently calculated. Infrared (IR) spectra were recorded in the 4000–500 $cm^{-1}$ range using spectroscopic-grade KBr pellets on a Nexus Thermo Nicolet FTIR spectrometer.

### *2.4. Electrochemical Study of Compounds in the Presence of $N_2$ and $CO_2$*

Electrochemical measurements were performed using a Biologic SP-300 potentiostat/galvanostat (Seyssinet-Pariset, France). Solutions were prepared at a concentration of 1 mM in dimethyl sulfoxide (DMSO) with 0.1 M tetrabutylammonium hexafluorophosphate ($TBAPF_6$) as the supporting electrolyte. A conventional three-electrode setup was used: a glassy carbon with a 3 mm diameter was employed as the working electrode, with a platinum wire as the counter electrode and a silver wire as the pseudo-reference electrode. All potentials were referenced to the $Fc/Fc^+$ redox couple in an external standard accordance with IUPAC rules [40,41]. Ohmic drop compensation was performed using positive feedback, with the Ru values measured via electrochemical impedance spectroscopy.

Cyclic voltammetry (CV) was performed at scan rates of 0.10, 0.25, 0.50, 0.75, 1.00, 1.50, and 2.00 V/s. The glassy carbon electrode was polished with 0.5 μm α-alumina on a Buehler 740 polishing cloth, rinsed with distilled water, and sonicated for 130 s. It was then rinsed again, dried, and cleaned before each measurement. The solutions were degassed by purging with nitrogen for 130 s prior to each experiment.

After characterizing the electrochemical behavior under $N_2$, the measurements were repeated under a $CO_2$ atmosphere. Experiments were conducted under identical conditions, except that the solutions were saturated with $CO_2$ via continuous bubbling. The cyclic voltammetry measurements focused on changes in the current and peak potentials at the same reversal potentials observed under $N_2$, which were attributed to molecular catalysis involving $CO_2$.

### *2.5. UV–Vis Spectroelectrochemical Study in the Presence of $N_2$ and $CO_2$*

A Thermo Scientific Evolution Array spectrophotometer (190–1000 nm) was coupled to a BioLogic SP-50 potentiostat/galvanostat (Seyssinet-Pariset, France). An optically transparent Au mesh was used as the working electrode, with a silver wire as the pseudo-reference electrode and a Pt wire as the auxiliary electrode. All electrodes were placed in a spectroelectrochemical quartz cell with an optical path length of 0.7 mm.

First, 1 mL of 0.2 mM $[Zn(2,2\text{-bpy})_3](BF_4)_2$ in DMSO containing 0.1 M $TBAPF_6$, previously purged with $N_2$, was added to the cell. UV–Vis spectra were recorded every 3 s for 3 min, while applying a constant potential of −1.88 V vs. $Fc/Fc^+$. The procedure was repeated using the same condition under a $CO_2$ atmosphere. Calibration of the spectrophotometer was performed using a standard holmium oxide, according to the equipment supplier.

### *2.6. Bulk Electrolysis in the Presence of $N_2$ and $CO_2$*

Bulk electrolysis experiments were performed using a Biologic SP-300 potentiostat/galvanostat connected to an electrolysis cell separated by a sintered glass frit. Glassy carbon cylinders were employed as both the working electrode and auxiliary electrode. A 10 mL solution containing 1 mM $[Zn(2,2\text{-bpy})_3](BF_4)_2$ in dimethyl sulfoxide (DMSO) with 0.1 M $TBAPF_6$ as the supporting electrolyte was electrolyzed under $N_2$ and $CO_2$ atmospheres by applying a potential of −2.3 V vs. Fc/Fc+ V for 15 min to achieve exhaustive electrolysis of the solution.

### *2.7. Identification of the Products*

To identify the products, gas chromatography (GC) and Fourier-transform infrared spectroscopy (FTIR) were employed. CO analysis was performed using a Thermo Scientific Trace 1300 gas chromatograph (Thermo Scientific, Madison, WI, USA). For each experiment, a 70 μL gas sample was injected through the injection port using a gas-tight syringe Hamilton (Reno, NV, USA). The injector and detector temperatures were set to 120 °C and 100 °C, respectively. For GC separation, the sample was introduced into the separation column and maintained at 50 °C with a split ratio of 30. Ultrapure helium was used as the carrier gas, at a flow rate of 5.0 mL $min^{-1}$. A TracePLOT TG-BOND Msieve 5A column (0.32 mm × 30 m) was employed for separation of the target gas component. Detection was performed using a thermal conductivity detector (TCD), and the chromatographic signals were recorded and analyzed using Chromeleon Software (Version 7.0). The data were processed via automated integration of the peak areas in the resolved chromatograms. FTIR measurements were carried out using a Shimadzu IRAffinity-1S spectrophotometer (Kyoto, Japan) equipped with an ATR module, in the spectral range of 4500 to 1000 $cm^{-1}$.

### 2.8. Theoretical Studies

Density functional theory (DFT) calculations were performed using the Gaussian 16 software package [42]. Full geometry optimizations were carried out without symmetry constraints, employing the B3LYP functional [43] and the LanL2DZ basis set [44], together with the SMD solvent model using DMSO as the solvent. These calculations were used to analyze the interaction between the zinc complex and $CO_2$ through the study of the electron transfer process involved. In particular, the quantum theory of atoms in molecules [45] was applied, using the molecular orbital set of each molecule to compute the atomic properties of the electron density with AIMAll software (Version 19.10.12) [46]. This analysis focused on the atomic population.

## 3. Results

### 3.1. Characterization of the Compound

To confirm ligand coordination and presence in the complexes, the compounds were first characterized using molar conductivity and infrared (FTIR) spectroscopy. The measured molar conductivity was 300 S $cm^2$ $mol^{-1}$, indicating that the $BF_4^-$ ions are located outside the coordination sphere [47].

The IR spectrum of the free ligand 2,2′-bipyridine (Figure S1, Supporting Information) exhibits vibrational bands corresponding to aromatic C–H stretching in the range of 3000–3100 $cm^{-1}$. Overtones (σ = CH) appear between 1600 and 2000 $cm^{-1}$, while the stretching bands (ν(C=C) + ν(C=N)) of the polypyridine rings are observed within the 1420–1640 $cm^{-1}$ range. Additionally, absorption bands associated with the out-of-plane C-H bending in the aromatic rings appear at 856 and 700 $cm^{-1}$ [48].

The IR spectrum of the $[Zn(2,2'\text{-bpy})_3](BF_4)_2$ complex (Figure S1b) retains the characteristic signals of the free ligand. Moreover, the appearance of an additional peak at 1060 $cm^{-1}$, attributed to the B–F stretching vibration, confirms the presence of the tetrafluoroborate anion in the complex [49].

### 3.2. Electrochemistry of $[Zn(2,2\text{-bpy})_3](BF_4)_2$ in the Absence and Presence of $CO_2$

Figure 2 shows the cyclic voltammetry of a 1 mM solution of $[Zn(2,2'\text{-bpy})_3](BF_4)_2$ in DMSO, recorded in the cathodic direction at a scan rate of 0.10 V/s. Two reduction processes, Ic and IIc, are observed, with a cathodic peak potential of Epc(I) = −1.93 V vs. $Fc/Fc^+$ and Epc (II) = −2.26 V vs. $Fc/Fc^+$. In the anodic direction, the corresponding oxidation peaks, Ia and IIa, appear at Epa(I) = −1.84 V vs. $Fc/Fc^+$ and Epa(II) = −2.18 V vs. $Fc/Fc^+$, respectively. From these values, the ΔE are determined to be $\Delta E_p$(I) = 0.060 V and $\Delta E_p$(II) = 0.080 V.

Figure 3 shows the cyclic voltametric response of a 1 mM $[Zn(2,2\text{-bpy})_3](BF_4)_2$ complex, with a normalized current ($i/v^{1/2}$) at different scan rates. The standard redox potentials are E° (I) = −1.88 V vs. $Fc/Fc^+$ and E°(II) = −2.22 V vs. $Fc/Fc^+$. These results indicate that both redox processes (I and II) exhibit fast diffusion-controlled electrode kinetics [15]. The variations in the current values of signals I and II are attributed to differences in the diffusion coefficients of the species involved in each process.

The experimental evidence supports an ErEr electrochemical mechanism (Equations (1) and (2)), indicating that the product of the first electron transfer undergoes a second electrochemical reduction. This complex exhibits low energy reorganization and can stabilize two reduced bipyridine ligands coordinated to Zn(II) [50,51].

$$[Zn(bpy)_3]^{2+} + 1e^- \rightarrow [Zn(bpy^-)(bpy)_2]^+ \quad (1)$$

$$[Zn(bpy^-)(bpy)_2]^+ + 1e^- \rightarrow [Zn(bpy)(bpy^-)_2] \quad (2)$$

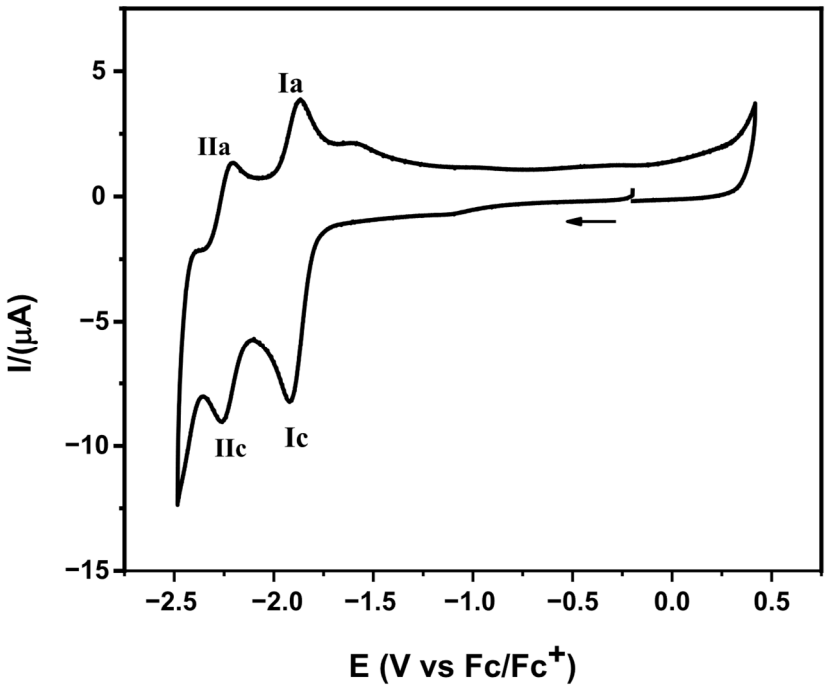



**Figure 2.** Cyclic voltametric response of a 1 mM [Zn (2,2-bpy)$_3$](BF$_4$)$_2$ in DMSO with 0.1 M TBAPF$_6$, recorded in the cathodic direction at a scan rate of 0.10 V/s under a $N_2$ atmosphere. The arrow indicates that the potential was initiated from OCP to negative direction.

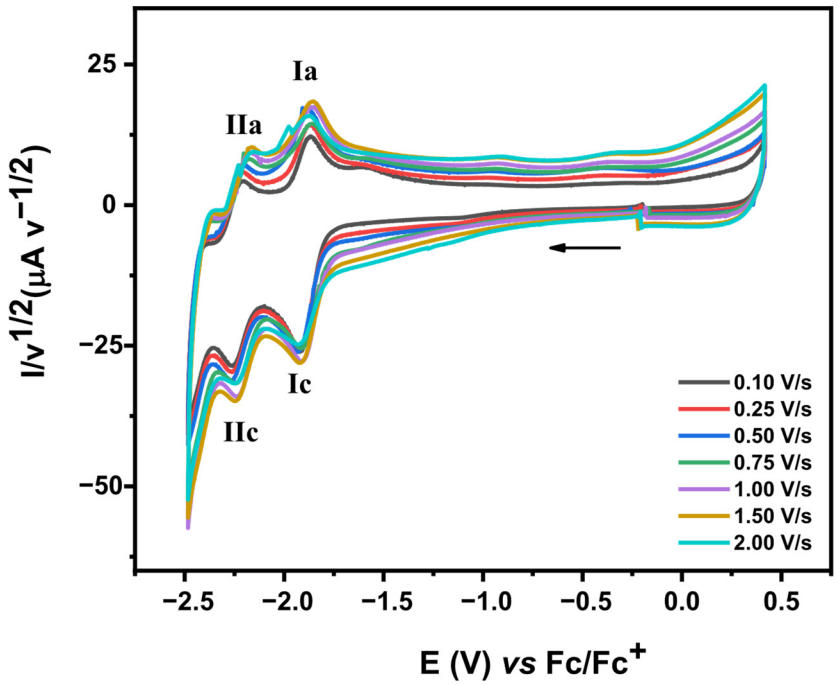



**Figure 3.** Normalized current cyclic voltametric response of 1 mM [Zn (2,2-bpy)$_3$](BF$_4$)$_2$ in DMSO with 0.1 M TBAPF$_6$ in the cathodic direction, under a $N_2$ atmosphere. The arrow indicates that the potential was initiated from OCP to a negative direction.

Cyclic voltammetry of 1 mM [Zn(2,2-bpy$_{)3}$](BF$_4$)$_2$ was also performed under identical conditions in the presence of $CO_2$. Figure 4 shows the resulting voltammogram, where two catalytic signals, Ik and IIk, appear at Epk(I) = −1.90 V vs. Fc/Fc$^+$ and Epk(II) = −2.18 V vs. Fc/Fc$^+$, respectively. Additionally, oxidation peaks Ia, Ia′, Ia″, and Ia‴ appear at −1.95, −1.72, −0.60, and −0.27 V vs. Fc/Fc$^+$, respectively. Except for the second oxidation

peak, these signals are attributed to the products formed during molecular $CO_2$ reduction catalyzed by the complex via an EC mechanism [15,52].

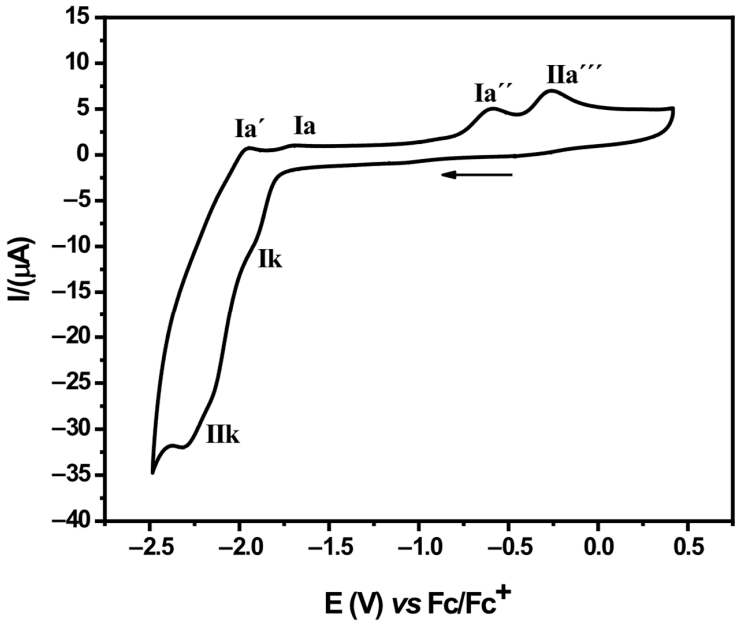



**Figure 4.** Cyclic voltametric response of a 1 mM $[Zn(2,2\text{-bpy})_3](BF_4)_2$ in DMSO with 0.1 M $TBAPF_6$, recorded in the cathodic direction at a scan rate of 0.10 V/s under a $CO_2$ atmosphere. The arrow indicates that the potential was initiated from OCP to a negative direction.

Figure 5 presents the cyclic voltametric responses recorded at different scan rates under a $CO_2$ atmosphere. The normalized currents ($i/v^{1/2}$) show values comparable to those observed under a $N_2$ atmosphere; however, a decrease in the intensity of the reduction product signals is evident upon $CO_2$ exposure. This suggests that molecular catalysis proceeds over a longer time window than the reversible electron transfer processes involving the diamine ligands.

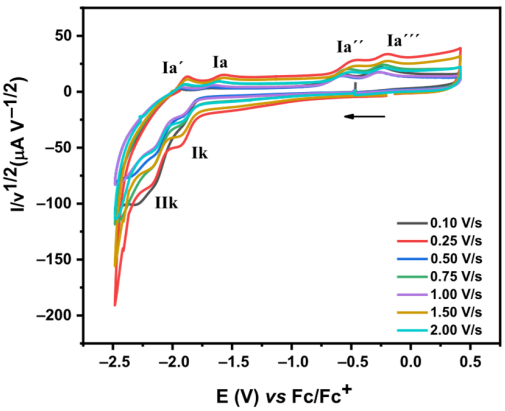



**Figure 5.** Normalized current cyclic voltametric response of 1 mM $[Zn(2,2\text{-bpy})_3](BF_4)_2$ in DMSO with 0.1 M $TBAPF_6$ in the cathodic direction, under a $CO_2$ atmosphere. The arrow indicates that the potential was initiated from OCP to a negative direction.

Figure 6 shows the comparative cyclic voltammetry response of 1 mM $[Zn(2,2\text{-bpy})_3](BF_4)_2$, recorded under $N_2$ and $CO_2$ atmospheres, at a scan rate of 0.10 V/s, under identical experimental conditions. The increase in current under $CO_2$ indicates the molecular catalysis of $CO_2$ reduction, with a more pronounced enhancement observed in the second reduction process (IIc) compared to the first (Ic).

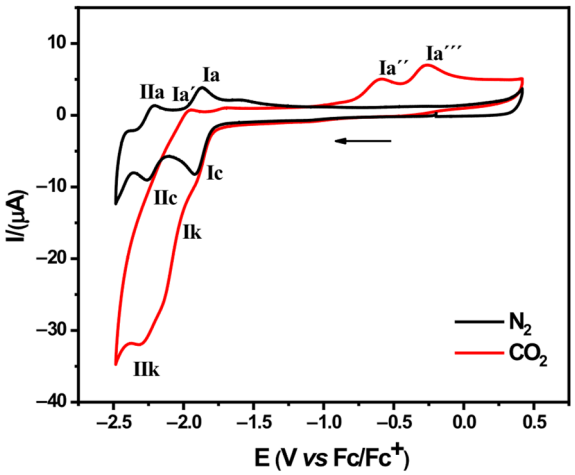



**Figure 6.** Comparative cyclic voltammetry response of 1 mM $[Zn(2,2\text{-bpy})_3](BF_4)_2$ in DMSO with $TBAPF_6$ 0.1 M under $N_2$ and $CO_2$ atmospheres, in the cathodic direction at 0.1 V/s. The arrow indicates that the potential was initiated from OCP to a negative direction.

Considering the stability of the electrochemically generated $[Zn(bpy^-)(bpy)_2]^+$ species, along with the ability of Zn(II) to adopt various coordination numbers and geometries [53], the following inner-sphere mechanism can be proposed, including the products formed during the process, see Equations (3)–(10):

Process Ik

$$[Zn(bpy)_3]^{2+} + 1e^- \rightarrow [Zn(bpy^-)(bpy)_2]^+ \quad (3)$$

$$[Zn(bpy^-)(bpy)_2]^+ + CO_2 \rightarrow [Zn(bpy)(bpy^-)(CO_2)]^+ + (bpy) \quad (4)$$

$$[Zn(bpy)(bpy^-)(CO_2)]^+ \rightarrow \left[Zn(bpy)_2(CO_2)^-\right]^+ \quad (5)$$

$$2\left[Zn(bpy)_2(CO_2)^-\right]^+ \rightarrow 2[Zn(bpy)_2]^{2+} + C_2O_4{}^{2-} \quad (6)$$

Process IIk

$$[Zn(bpy)_2]^{2+} + 1e^- \rightarrow [Zn(bpy)(bpy^-)]^+ \quad (7)$$

$$[Zn(bpy)(bpy^-)]^+ + CO_2 \rightarrow [Zn(bpy)(bpy^-)(CO_2)]^+ \quad (8)$$

$$[Zn(bpy)(bpy^-)(CO_2)]^+ \rightarrow \left[Zn(bpy)_2(CO_2)^-\right]^+ \quad (9)$$

$$2\left[Zn(bpy)_2(CO_2)^-\right]^+ \rightarrow 2[Zn(bpy)_2]^{2+} + C_2O_4{}^{2-} \quad (10)$$

To confirm the product of this mechanism, bulk electrolysis of a 1 mM solution of $[Zn(2,2\text{-bpy})_3](BF_4)_2$ in DMSO containing 0.1 M $TBAPF_6$ as the supporting electrolyte was performed under both $N_2$ and $CO_2$ atmospheres. Notably, under a $N_2$ atmosphere, the electrolyzed solution changed to a pale purple color, whereas, under $CO_2$, no color change was observed. This suggests that different pathways are observed in both atmospheres. To analyze the formation of products from $[Zn(2,2\text{-bpy})_3](BF_4)_2$ electrolyzed under $CO_2$, GC analysis was performed, where no signal of CO was detected. In contrast, the FTIR spectrum (Figure S2) after bulk electrolysis showed bands at 1640 at 1350 $cm^{-1}$ and 1270 $cm^{-1}$ related to C=O stretching, C-O and C-C stretching. These signals confirm the formation of oxalate, consistent with the literature reports [26,54,55].

From the cyclic voltammograms, foot of the wave analysis (FOWA) [56,57] was performed for the reduction process Ic of the complex $[Zn(2,2\text{-bpy})_3](BF_4)_2$, as shown in Figure 7, according to the plot:

$$\frac{i}{i_p^\circ} vs \frac{1}{1+\exp\left[\frac{R}{RT}\left(E-E^\circ\frac{ML_{red}}{ML_{ox}}\right)\right]}.$$

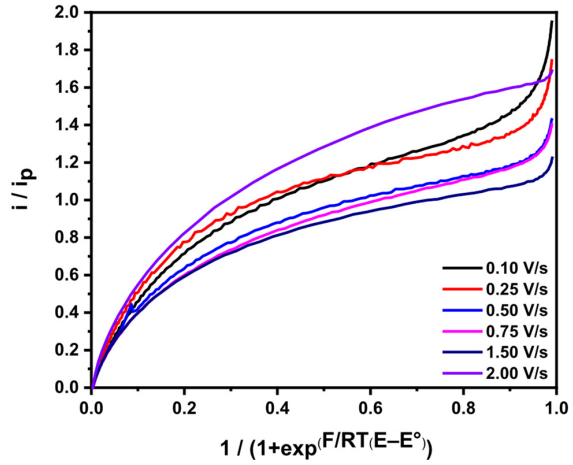



**Figure 7.** Foot of the wave analysis (FOWA) of the 1 mM $[Zn(2,2'\text{-bpy})_3](BF_4)_2$ complex in DMSO with 0.1 M $TBAPF_6$ as the supporting electrolyte.

The slope of the plot allows the calculation of the catalytic rate constant ($k$), which corresponds to $1.352 \times 10^3$ $M^{-1}{\cdot}s^{-1}$ (Figure 8). This value is higher than the reported values of $1.220 \times 10^2$ $M^{-1}{\cdot}s^{-1}$ for $[Co(2,2\text{-bpy})_3]^{2+}$ and $8.7 \times 10^2$ $M^{-1}{\cdot}s^{-1}$ for $[Fe(2,2\text{-bpy})_3]^{2+}$ in the references [25,58].

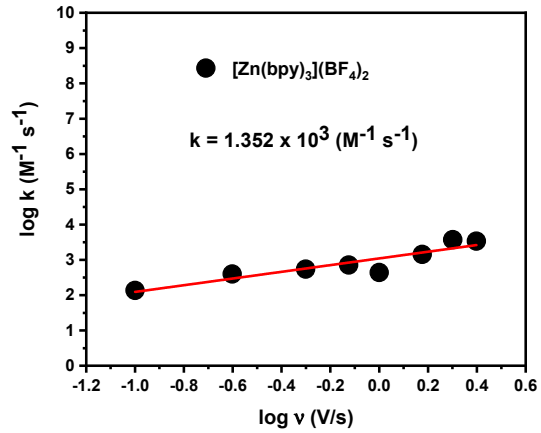



**Figure 8.** Logarithmic rate constant ($k$) obtained from foot of the wave analysis (FOWA) of the 1 mM $[Zn(2,2'\text{-bpy})_3](BF_4)_2$ complex in DMSO with 0.1 M $TBAPF_6$ as the supporting electrolyte.

### *3.3. UV–Vis Spectroelectrochemical Response of the Complex [Zn (2,2-bpy)$_3$](BF$_4$)$_2$ in the Absence and Presence of CO$_2$*

UV–Vis spectroelectrochemical experiments were carried out using a 0.2 mM solution of $[Zn(2,2\text{-bpy})_3](BF_4)_2$ in MeCN with 0.1 M $TBAPF_6$ under a $N_2$ atmosphere. A gold mesh was employed as the working electrode, and chronoamperometric measurements were performed by applying a constant potential of −1.88 vs. $Fc/Fc^+$. Simultaneously, UV–Vis spectra were recorded every 3 s during electrolysis at the electrode surface over a period of 3 min as shown in Figure 9.

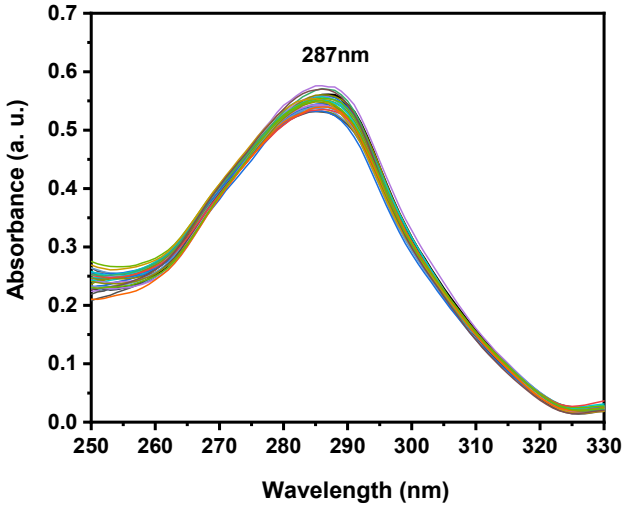



**Figure 9.** UV–Vis spectroelectrochemical response of 0.2 mM of the $[Zn(2,2'\text{-bpy})_3](BF_4)_2$ complex in DMSO with 0.1 M $TBAPF_6$ as the supporting electrolyte under a $N_2$ atmosphere. A potential of −1.88 V vs. $Fc/Fc^+$ was applied, and UV–Vis spectra were recorded every 3 s over a period of 3 min. Each color line represents a measurement at different sample time.

The absorbance band at 287 nm, associated with the ligand [59], remained stable throughout the experiment, as illustrated in Figure S3. Conversely, under the $CO_2$ atmosphere (Figure 10), a slight increase in absorbance, a small hypochromic shift, and band narrowing were observed (Figure S4). These modifications suggest an interaction between $CO_2$ and the reduced species formed during the electrolysis [25]. Additionally, at a wavelength of 315 nm, an isosbestic point can be observed, indicating the formation of new bond that modifies the structure of the Zn(II) coordination compound. This phenomenon is likely associated with a change in the coordination sphere upon $CO_2$ binding to the ternary Zn(II) complex.

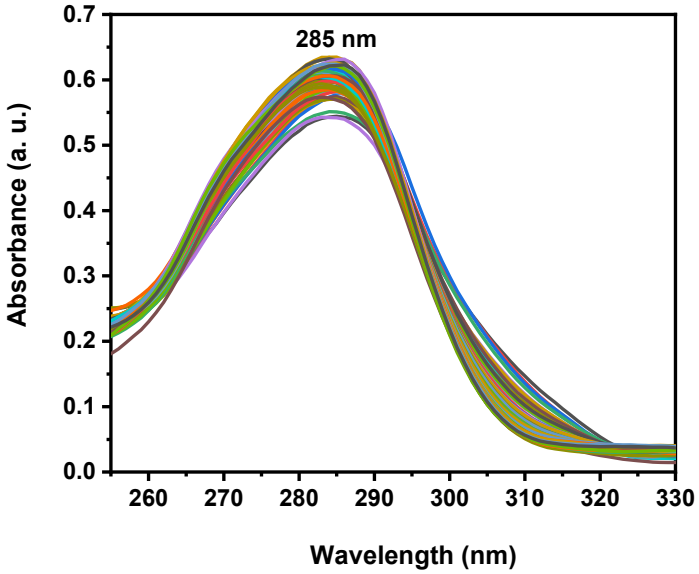



**Figure 10.** UV–Vis spectroelectrochemical response of 0.2 mM of the $[Zn(2,2'\text{-bpy})_3](BF_4)_2$ complex in DMSO with 0.1 M $TBAPF_6$ as the supporting electrolyte under a $CO_2$ atmosphere. A potential of −1.88 V vs. $Fc/Fc^+$ was applied, and UV–Vis spectra were recorded every 3 s over a period of 3 min. Each color line represents a measurement at different sample time.

Furthermore, the formation of the anionic species follows an exponential trend consistent with first-order kinetics [60]. Based on this observation, the data were fitted to a first-order kinetic model, yielding a rate constant of 0.0069 $s^{-1}$ (Figure S5).

### *3.4. Theoretical Calculations and Their Correlation with Redox Processes*

The LUMOs of the chemical species $[Zn(bpy)_3]^{2+}$ and $[Zn(bpy)_3]^{+}$ are presented in Figure 11. In both cases, the electron density is primarily localized on the ligands, consistent with the electrochemical mechanism proposed in Section 3.2. The calculated LUMO energies are −0.21367 eV for $[Zn(bpy)_3]^{2+}$ (Figure 11a) and −0.12522 eV for $[Zn(bpy)_3]^{+}$ (Figure 11b), indicating a significant ligand contribution to the electron density and suggesting that the ligands play a crucial role in the $CO_2$ reduction mechanism.

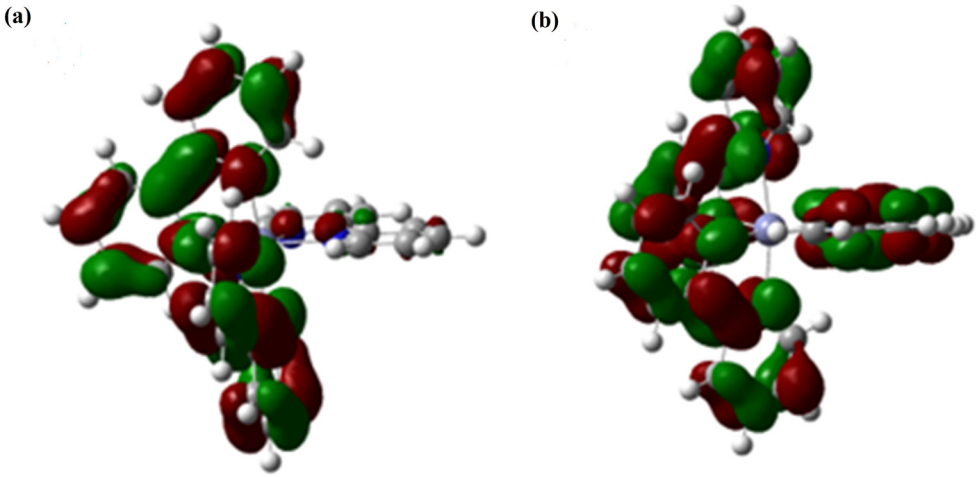



**Figure 11.** Lowest unoccupied molecular orbital (LUMO) of the cationic species (**a**) $[Zn(bpy)_3]^{2+}$ and (**b**) $[Zn(bpy)_3]^{+}$.

The interaction between $CO_2$ and $[Zn(bpy)_3]^{2+}$ was analyzed via the energy and population changes when the $CO_2$ molecule approached the zinc center. Figure 12 shows the structural changes related to the coordination of a $CO_2$ molecule with the $[Zn(bpy)_3]^{2+}$ complex. In Figure 12a, the Zn-O($CO_2$) bond distance is 5.5208 Å, and the complex exhibits an octahedral geometry, while in Figure 12b, the Zn-O($CO_2$) bond distance is 2.2208 Å; now, the $CO_2$ occupies the apical position at the octahedral geometry and displaces one nitrogen atom from a bipyridine ligand. The change in coordination sphere of the zinc metal for the ligand displacement is consistent with the discussion of the UV–Vis results in the previous section, related to the UV–Vis spectroelectrochemical response of the complex.

Figure 13 shows the energy change when the $CO_2$ molecule approaches the $[Zn(bpy)_3]^{2+}$ complex from 5.5208 to 2.2208 Å and is coordinated with the metal center. The energetic value related to the coordination process for the $CO_2$ molecule to the Zn metal and displacement of one bipyridine nitrogen atom is 22.4 kcal/mol.

Figure 14 shows the population change for the same process at the zinc atom, the sum of the atoms in the three bipyridine ligands, and the sum of the $CO_2$ atoms. It is observed that when $CO_2$ moves closer to the complex, the zinc and the carbon dioxide lose population, −0.031 $e^-$ and −0.003 $e^-$, respectively, while the ligands gain population, 0.034 $e^-$. At this point, the oxygen atom moved from the $CO_2$ nearer to the Zn gained population (0.05 $e^-$) when it was coordinated with the apical position of the complex and replaced the nitrogen atom. Once the Zn-O bond was formed, the ligands recovered the electron density previously shared with the metal; this result supports the importance of the ligand in the $CO_2$ reduction process. The electrochemical (Section 3.2) and spectroelectrochemical (Section 3.3) studies in the presence of $CO_2$, where the shift potential in cyclic voltammetry

and the absorption maximum in UV–Vis spectroelectrochemical are presented, allow us to propose the $CO_2$ coordination with the metal center.

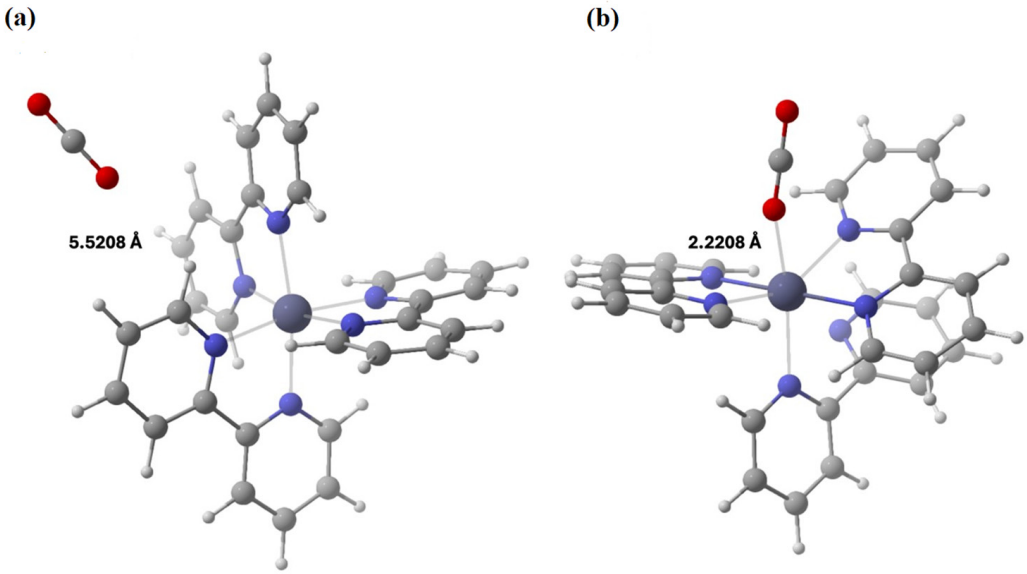



**Figure 12.** Change in coordination sphere for the $[Zn(bpy)_3]^{2+}$ complex when the (**a**) $CO_2$ molecule is far away and (**b**) when it is coordinated with the zinc atom. Carbon atoms are in grey, hydrogen atoms in white, oxygen atoms in red, nitrogen atoms in blue and zinc atoms in dark grey.

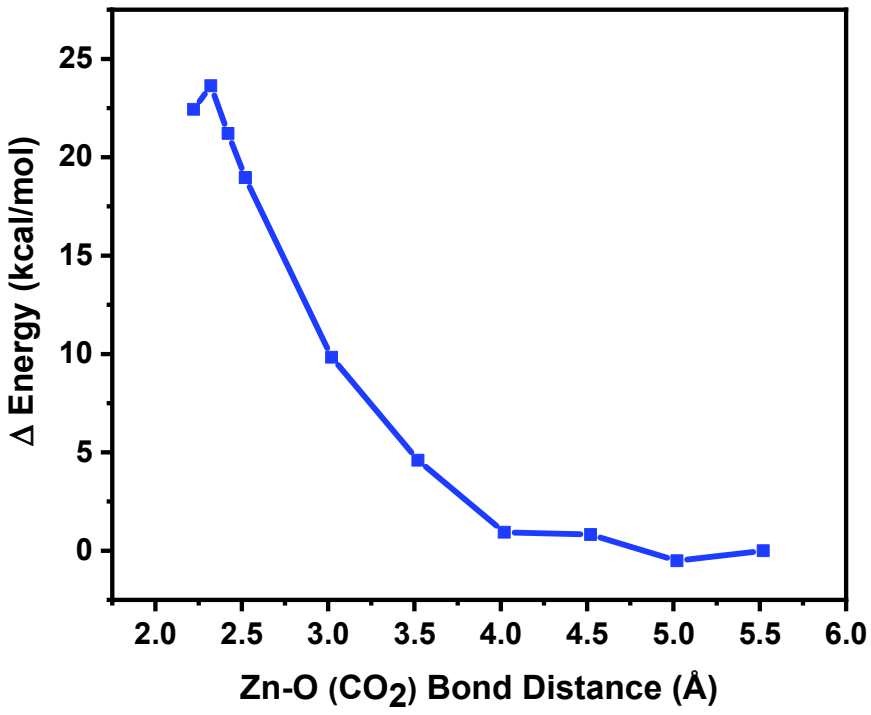



**Figure 13.** Energy change in the function of the $[Zn(bpy)_3]^{2+}$–$CO_2$ distance.

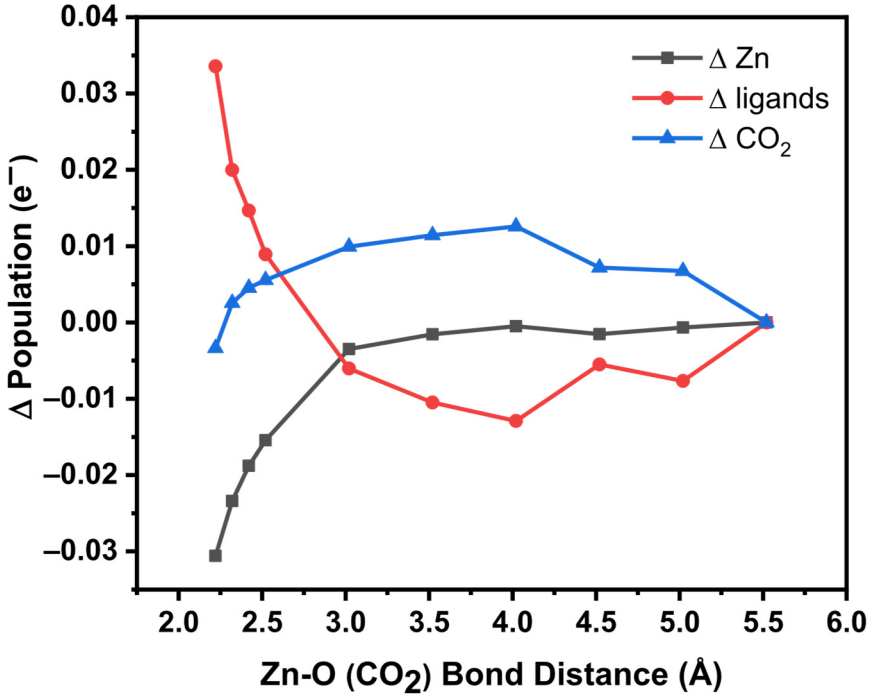



**Figure 14.** Population change for the Zn metal center (black line) and bipyridine ligands (red line) when the $CO_2$ (blue line) reaches the $[Zn(bpy)_3]^{2+}$ complex.

## 4. Conclusions

Electrochemical techniques were employed to elucidate the reduction mechanism of the $[Zn(2,2\text{-bpy})_3](BF_4)_2$ complex, revealing that, at highly cathodic potentials, the inner-sphere reduction of the 2,2′-bipyridine ligands occurs. Moreover, the complex's electrochemical response in the presence of $CO_2$ confirms its role in molecular catalysis. The octahedral $[Zn(2,2\text{-bpy})_3](BF_4)_2$ complex exhibits notable catalytic efficiency, as evidenced by its cyclic voltammetry response under a $CO_2$ atmosphere and quantified by a catalytic constant of $k = 1.352 \times 10^3\ M^{-1}{\cdot}s^{-1}$. Complementary spectroelectrochemical experiments and DFT calculations demonstrate the interaction of the complex with $CO_2$, while bulk electrolysis and FTIR analysis suggest that oxalate is the main product of the catalytic $CO_2$ reduction.

**Supplementary Materials:** The following supporting information can be downloaded at: https://www.mdpi.com/article/10.3390/pr13113443/s1, Figure S1: (a) FT-IR spectrum of 2,2-bipyridine; (b) FT-IR spectrum of [Zn (2,2-bpy)3](BF4)2; Figure S2: FT-IR spectrum of [Zn (2,2-bpy)3](BF4)2 electrolyzed in presence of CO2.; Figure S3: Comparative UV-Vis spectra showing the first and last recorded spectra from the UV-Vis spectroelectrochemical response of 0.2 mM [Zn (2,2-bpy)3](BF4)2 in DMSO containing 0.1 M TBAPF6 under $N_2$ atmosphere. A potential of −1.88 V vs. $Fc/Fc^+$ was applied; Figure S4: Comparative UV-Vis spectra showing the first and last recorded spectra from the UV-Vis spectroelectrochemical response of 0.2 mM [Zn (2,2-bpy)3](BF4)2 in DMSO containing 0.1 M TBAPF6 under $CO_2$ atmosphere. A potential of −1.88 V vs $Fc/Fc^+$ was applied; Figure S5: Comparative plot of time vs. Δabsorbance at 283 and 286 nm for the UV-Vis spectroelectrochemical response of 0.2 mM [Zn (2,2-bpy)3](BF4)2 in DMSO containing 0.1 M TBAPF6 under $CO_2$ and $N_2$ atmospheres. A potential of −1.88 V vs. $Fc/Fc^+$ was applied.

**Author Contributions:** Conceptualization, G.R.-O., J.P.F.R.-C. and L.O.-F.; Method-ology, G.R.-O., B.M.L.-M., L.G.T.-C., F.C.-G., J.P.F.R.-C. and G.H.-P.; Software, F.C.-G. and J.P.F.R.-C.; Validation, J.P.F.R.-C., L.G.R.-P. and M.C.-R.; Formal analysis, G.R.-O., B.M.L.-M., J.P.F.R.-C. and L.G.R.-P.; Investigation, G.R.-O. and L.G.T.-C.; Resources, L.O.-F.; Data curation, G.R.-O. and L.G.T.-C.; Writing—original draft, G.R.-O., L.G.T.-C., J.P.F.R.-C., L.G.R.-P. and M.C.-R.; Writing—review and

editing, G.R.-O., L.G.T.-C., J.P.F.R.-C., G.H.-P., L.G.R.-P. and M.C.-R.; Visualization, J.P.F.R.-C., L.G.R.-P. and M.C.-R.; Supervision, L.O.-F.; Project administration, L.O.-F.; Funding acquisition, L.O.-F. All authors have read and agreed to the published version of the manuscript.

**Funding:** This research was funded by "Secretaria de Ciencia Humanidades Tecnología e Innovación SECIHTI", "Ciencia Básica y de Frontera 2023–2024", Grant number CBF2023-2024-3108 and CONACyT-Apoyo a la Infraestructura 2016 (269102) and Secretaria de Ciencia Humanidades Tecnología e Innovación SECIHTI".

**Data Availability Statement:** The original contributions presented in this study are included in the article and Supplementary Materials. Further inquiries can be directed to the corresponding author.

**Acknowledgments:** The authors thank DGTIC-UNAM (LANCAD-UNAM-DGTIC-194) for the computer time. G.R.-O. expresses gratitude to SECIHTI for the scholarship 6364841 provided through the program: Estancias Posdoctorales por México 2023. L.G.T.-C. acknowledges the scholarship granted to CVU 689679 through the Postdoctoral Fellowship program "Por México" 2024. The authors declare that generative AI tools (ChatGPT 4.0) was used solely for improving the clarity and grammar of the manuscript text. Additionally, AI-assisted tools (OpenAI, San Francisco, CA, USA) was used to generate the graphical abstract image. No AI tools were used to produce scientific content, data, analyses, or references. The authors take full responsibility for the accuracy and integrity of the content of this publication.

**Conflicts of Interest:** The authors declare that they have no known competing financial interests or personal relationships that could have appeared to influence the work reported in this paper.

## References

1. Core Writing Team; Lee, H.; Romero, J. (Eds.) Summary for Policymakers. In *Climate Change 2023: Synthesis Report*; Contribution of Working Groups I, II and III to the Sixth Assessment Report of the Intergovernmental Panel on Climate Change IPCC; Intergovernmental Panel on Climate Change IPCC: Geneva, Switzerland, 2023; pp. 1–34. [CrossRef]
2. Dunstone, N.J.; Smith, D.M.; Atkinson, C.; Colman, A.; Folland, C.; Hermanson, L.; Ineson, S.; Killick, R.; Morice, C.; Rayner, N.; et al. Will 2024 be the first year that global temperature exceeds 1.5 °C? *Atmos. Sci. Lett.* **2024**, *25*, e1254. [CrossRef]
3. Crippa, M.; Guizzardi, D.; Pagani, F.; Banja, M.; Muntean, M.; Schaaf, E.; Monforti-Ferrario, F.; Becker, W.E.; Quadrelli, R.; Risquez-Martin, A.; et al. *GHG Emissions of All World Countries*; European Union: Luxembourg, 2024. [CrossRef]
4. Sanabria, E.; Maldonado, M.; Matiz, C.; Ribeiro, A.C.F.; Esteso, M.A. Methods of capture and transformation of carbon dioxide ($CO_2$) with macrocycles. *Processes* **2025**, *13*, 117. [CrossRef]
5. Xu, J.; Zhong, G.; Li, M.; Zhao, D.; Sun, Y.; Hu, X.; Sun, J.; Li, X.; Zhu, W.; Li, M.; et al. Review on electrochemical carbon dioxide capture and transformation with bipolar membranes. *Chin. Chem. Lett.* **2023**, *34*, 108075. [CrossRef]
6. Thoi, V.S.; Sun, Y.; Long, J.R.; Chang, C.J. Complexes of earth-abundant metals for catalytic electrochemical hydrogen generation under aqueous conditions. *Chem. Soc. Rev.* **2013**, *42*, 2388–2400. [CrossRef]
7. Rountree, E.S.; McCarthy, B.D.; Eisenhart, T.T.; Dempsey, J.L. Evaluation of homogeneous electrocatalysts by cyclic voltammetry. *Inorg. Chem.* **2014**, *53*, 9983–10002. [CrossRef]
8. Sun, Z.; Ma, T.; Tao, H.; Fan, Q.; Han, B. Fundamentals and challenges of electrochemical $CO_2$ reduction using two-dimensional materials. *Chem* **2017**, *3*, 560–587. [CrossRef]
9. Yadav, P.K.; Kumari, N.; Pachfule, P.; Banerjee, R.; Mishra, L. Metal [Zn(II), Cd(II)], 1,10-phenanthroline containing coordination polymers constructed on the skeleton of polycarboxylates: Synthesis, characterization, microstructural, and $CO_2$ gas adsorption studies. *Cryst. Growth Des.* **2012**, *12*, 5311–5319. [CrossRef]
10. Schrodt, A.; Neubrand, A.; van Eldik, R. Fixation of $CO_2$ by Zinc(II) Chelates in Alcoholic Medium. X-ray Structures of $\{[Zn(cyclen)]_3(\mu_3\text{-}CO_3)\}(ClO_4)_4$ and $[Zn(cyclen)EtOH](ClO_4)_2$. *Inorg. Chem.* **1997**, *36*, 4579–4584. [CrossRef] [PubMed]
11. Chiericato, G.; Arana, C.R.; Casado, C.; Cuadrado, I.; Abruña, H.D. Electrocatalytic reduction of carbon dioxide mediated by transition metal complexes with terdentate ligands derived from diacetylpyridine. *Inorganica Chim. Acta* **2000**, *300–302*, 32–42. [CrossRef]
12. Cao, Y.; Chen, Q.; Shen, C.; He, L. Polyoxometalate-based catalysts for $CO_2$ conversion. *Molecules* **2019**, *24*, 2069. [CrossRef]
13. Schwarz, H.A.; Creutz, C.; Sutin, N. Homogeneous catalysis of the photoreduction of water by visible light. 4. Cobalt(I) polypyridine complexes. Redox and substitutional kinetics and thermodynamics in the aqueous 2,2′-bipyridine and 4,4′-dimethyl-2,2′-bipyridine series studied by the pulse-radiolysis technique. *Inorg. Chem.* **1985**, *24*, 433–439. [CrossRef]

14. Amatore, C.; Saveant, J.M. Mechanism and kinetic characteristics of the electrochemical reduction of carbon dioxide in media of low proton availability. *J. Am. Chem. Soc.* **1981**, *103*, 5021–5023. [CrossRef]
15. Savéant, J.-M. Molecular catalysis of electrochemical reactions. mechanistic aspects. *Chem. Rev.* **2008**, *108*, 2348–2378. [CrossRef]
16. Berardi, S.; Drouet, S.; Francàs, L.; Gimbert-Suriñach, C.; Guttentag, M.; Richmond, C.; Stoll, T.; Llobet, A. Molecular artificial photosynthesis. *Chem. Soc. Rev.* **2014**, *43*, 7501–7519. [CrossRef] [PubMed]
17. Benson, E.E.; Kubiak, C.P.; Sathrum, A.J.; Smieja, J.M. Electrocatalytic and homogeneous approaches to conversion of $CO_2$ to liquid fuels. *Chem. Soc. Rev.* **2009**, *38*, 89–99. [CrossRef] [PubMed]
18. Feng, D.-M.; Zhu, Y.-P.; Chen, P.; Ma, T.-Y. Recent advances in transition-metal-mediated electrocatalytic $CO_2$ reduction: From homogeneous to heterogeneous systems. *Catalysts* **2017**, *7*, 373. [CrossRef]
19. Han, J.; Wang, N.; Li, X.; Lei, H.; Wang, Y.; Guo, H.; Jin, X.; Zhang, Q.; Peng, X.; Zhang, X.-P.; et al. Bioinspired Iron Porphyrins with appended poly-pyridine/amine units for boosted electrocatalytic $CO_2$ reduction reaction. *eScience* **2022**, *2*, 623–631. [CrossRef]
20. Boutin, E.; Merakeb, L.; Ma, B.; Boudy, B.; Wang, M.; Bonin, J.; Anxolabéhère-Mallart, E.; Robert, M. Molecular catalysis of $CO_2$ reduction: Recent advances and perspectives in electrochemical and light-driven processes with selected Fe, Ni and Co aza macrocyclic and polypyridine complexes. *Chem. Soc. Rev.* **2020**, *49*, 5772–5809. [CrossRef]
21. Bonin, J.; Robert, M.; Routier, M. Selective and efficient photocatalytic $CO_2$ reduction to CO using visible light and an iron-based homogeneous catalyst. *J. Am. Chem. Soc.* **2014**, *136*, 16768–16771. [CrossRef] [PubMed]
22. Bi, J.; Hou, P.; Liu, F.; Kang, P. Electrocatalytic reduction of $CO_2$ to methanol by iron tetradentate phosphine complex through amidation strategy. *ChemSusChem* **2019**, *12*, 2195–2201. [CrossRef]
23. Juris, A.; Balzani, V.; Barigelletti, F.; Campagna, S.; Belser, P.; von Zelewsky, A. Ru(II) polypyridine complexes: Photophysics, photochemistry, eletrochemistry, and chemiluminescence. *Coord. Chem. Rev.* **1988**, *84*, 85–277. [CrossRef]
24. Simpson, T.C.; Durand, R.R. Ligand participation in the reduction of $CO_2$ catalyzed by complexes of 1,10 o-Phenanthroline. *Electrochim. Acta* **1988**, *33*, 581–583. [CrossRef]
25. Rocha-Ortiz, G.; Barrios-Velasco, A.; Zúñiga, O.M.; Cruz-Ramírez, M.; Mendoza, A.; Ramírez-Palma, L.G.; Rebolledo-Chávez, J.P.F.; Ortiz-Frade, L. The Role of Geometry in Cobalt–Polypyridine Complexes in the Electrochemical Reduction of $CO_2$ Using UV-Vis Spectroelectrochemistry. *Catalysts* **2025**, *15*, 641. [CrossRef]
26. Rebolledo-Chávez, J.P.F.; Toral, G.T.; Ramírez-Delgado, V.; Reyes-Vidal, Y.; Jiménez-González, M.L.; Cruz-Ramírez, M.; Mendoza, A.; Ortiz-Frade, L. The Role of Redox Potential and Molecular Structure of Co(II)-Polypyridine Complexes on the Molecular Catalysis of $CO_2$ Reduction. *Catalysts* **2021**, *11*, 948. [CrossRef]
27. Elgrishi, N.; Chambers, M.B.; Wang, X.; Fontecave, M. Molecular polypyridine-based metal complexes as catalysts for the reduction of $CO_2$. *Chem. Soc. Rev.* **2017**, *46*, 761–796. [CrossRef]
28. Elgrishi, N.; Chambers, M.B.; Artero, V.; Fontecave, M. Terpyridine complexes of first row transition metals and electrochemical reduction of $CO_2$ to CO. *Phys. Chem. Chem. Phys.* **2014**, *16*, 13635–13644. [CrossRef] [PubMed]
29. Ling, Z.; Yin, Y.; Kang, X.; Li, X.; Duan, R.; Zhou, S.; Liu, H.; Mo, G.; Chen, Z.; Wu, X.; et al. Enhanced electrochemical reduction of $CO_2$ to CO by ZnO nanorods enriched with oxygen vacancies. *Chem Catal.* **2025**, *5*, 101192. [CrossRef]
30. Xue, L.; Zhang, C.; Shi, T.; Liu, S.; Zhang, H.; Sun, M.; Liu, F.; Liu, Y.; Wang, Y.; Gu, X.; et al. Unraveling the improved $CO_2$ adsorption and COOH* formation over Cu-decorated ZnO nanosheets for $CO_2$ reduction toward CO. *Chem. Eng. J.* **2023**, *452*, 139701. [CrossRef]
31. Ma, X.; Jiao, D.; Fan, J.; Dong, Y.; Cui, X. Metal–oxide heterointerface synergistic effects of copper–zinc systems for highly selective $CO_2$-to-$CH_4$ electrochemical conversion. *Inorg. Chem. Front.* **2023**, *10*, 168–173. [CrossRef]
32. Yan, J.-C.; Wang, F.-M.; Yin, S.; Zhang, J.; Jiang, W.; Liu, G.-G. Copper/metal oxide heterostructures for electrochemical carbon dioxide reduction. *Rare Met.* **2025**, *44*, 2239–2267. [CrossRef]
33. Nakazato, R.; Matsumoto, K.; Quintelier, M.; Rosero-Navarro, N.C.; Miura, A.; Tadanaga, K. $CO_2$ electrochemical reduction by Zn-based layered double hydroxides: The role of structural trivalent metal ions. *Open Ceram.* **2025**, *22*, 100788. [CrossRef]
34. Wang, B.; Wang, L.; Lin, J.; Xia, C.; Sun, W. Multifunctional Zn-N4 Catalysts for the Coupling of $CO_2$ with Epoxides into Cyclic Carbonates. *ACS Catal.* **2023**, *13*, 10386–10393. [CrossRef]
35. Wu, Y.; Jiang, J.; Weng, Z.; Wang, M.; Broere, D.L.J.; Zhong, Y.; Brudvig, G.W.; Feng, Z.; Wang, H. Electroreduction of $CO_2$ Catalyzed by a Heterogenized Zn–Porphyrin Complex with a Redox-Innocent Metal Center. *ACS Cent. Sci.* **2017**, *3*, 847–852. [CrossRef]
36. Fang, Y.; Hong, X.; Fu, Y.; Li, Y.; Chao, D. Ligand-based electron transfer enables molecular polypyridyl Zn(II) complexes for efficient photocatalytic $CO_2$ reduction. *Mol. Catal.* **2023**, *551*, 113610. [CrossRef]
37. Stamatelos, I.; Dinh, C.-T.; Lehnert, W.; Pasel, J.; Shviro, M. Zn-based catalysts for selective and stable electrochemical $CO_2$ reduction at high current densities. *ACS Appl. Energy Mater.* **2022**, *5*, 13928–13938. [CrossRef]
38. Norouziyanlakvan, S.; Berro, P.; Rao, G.K.; Gabidullin, B.; Richeson, D. Electrocatalytic Reduction of $CO_2$ and $H_2O$ with Zn(II) Complexes Through Metal–Ligand Cooperation. *Chem. Eur. J.* **2024**, *30*, e202303147. [CrossRef]

39. Costentin, C.; Robert, M.; Saveant, J.-M. Catalysis of the electrochemical reduction of carbon dioxide. *Chem. Soc. Rev.* **2013**, *42*, 2423–2436. [CrossRef] [PubMed]
40. Trasatti, S. The Absolute Electrode Potential: An Explanatory Note (Recommendations 1986). *Pure Appl. Chem.* **1986**, *58*, 955–966. [CrossRef]
41. Gagne, R.R.; Koval, C.A.; Lisensky, G.C. Ferrocene as an internal standard for electrochemical measurements. *Inorg. Chem.* **1980**, *19*, 2854–2855. [CrossRef]
42. *Gaussian 16, Revision C.01*; Frisch, M.J., Trucks, G.W., Schlegel, H.B., Scuseria, G.E., Robb, M.A., Cheeseman, J.R., Scalmani, G., Barone, V., Petersson, G.A., Nakatsuji, H., et al., Eds.; Gaussian, Inc.: Wallingford, CT, USA, 2016.
43. Becke, A.D. Density-functional thermochemistry. III. The role of exact exchange. *J. Chem. Phys.* **1993**, *98*, 5648–5652. [CrossRef]
44. Dunning, T.H., Jr.; Hay, P.J. *Modern Theoretical Chemistry*; Schaefer, H.F., III, Ed.; Plenum: New York, NY, USA, 1977; Volume 3, pp. 1–28.
45. Bader, R. *Atoms in Molecules: A Quantum Theory*; Oxford University Press: New York, NY, USA, 1990. [CrossRef]
46. Keith, T.A. *AIMAll*, version 16.01.09; TK Gristmill Software: Overland Park, KS, USA, 2016. Available online: https://aim.tkgristmill.com/ (accessed on 15 September 2025).
47. Greenwood, N.N.; Earnshaw, A. *Chemistry of the Elements*, 2nd ed.; Butterworth-Heinemann: Oxford, UK, 2017; pp. 1–1376.
48. Willard, H.H.; Eroles Gómez, A. *Métodos Instrumentales de Análisis*; CECSA: Coahuila, Mexico, 1990; pp. 1–907.
49. Zhang, Z.; Zhang, Z.; Hao, B.N.; Zhang, H.; Wang, M.; Liu, Y.D. Fabrication of imidazolium-based poly(ionic liquid) microspheres and their electrorheological responses. *J. Mater. Sci.* **2017**, *52*, 5778–5787. [CrossRef]
50. Kadirov, M.K.; Kholin, K.V.; Tselishcheva, E.Y.; Burilov, V.A.; Mustafina, A.R. Cyclic voltammetry of tris(2,2′-bipyridine)zinc(II) diperchlorate detected by Electron Spin Resonance. *Russ. Chem. Bull.* **2013**, *62*, 1327–1331. [CrossRef]
51. Müller, I.; Schneider, C.; Pietzonka, C.; Kraus, F.; Werncke, C.G. Reduction of 2,2′-bipyridine by quasi-linear 3D-metal(I) silylamides—A structural and spectroscopic study. *Inorganics* **2019**, *7*, 117. [CrossRef]
52. Lacy, D.C.; McCrory, C.C.L.; Peters, J.C. Studies of Cobalt-mediated electrocatalytic $CO_2$ reduction using a redox-active ligand. *Inorg. Chem.* **2014**, *53*, 4980–4988. [CrossRef]
53. Desbouis, D.; Troitsky, I.P.; Belousoff, M.J.; Spiccia, L.; Graham, B. Copper(II), zinc(II) and nickel(II) complexes as nuclease mimetics. *Coord. Chem. Rev.* **2012**, *256*, 897–937. [CrossRef]
54. Kim, S.-M.; Yoon, I.-H.; Kim, I.-G.; Park, C.W.; Sihn, Y.; Kim, J.-H.; Park, S.-J. Cs desorption behavior during hydrothermal treatment of illite with oxalic acid. *Environ. Sci. Pollut. Res.* **2020**, *27*, 35580–35590. [CrossRef]
55. Rocha-Ortiz, G.; González-Gutiérrez, A.G.; Casillas-Santana, N.; Astudillo-Sánchez, P.D.; Romero-Arellano, V.H.; Blancas-Flores, J.M. Innovative dielectric polyaniline composites for performance triboelectric nanogenerators. *J. Solid State Electrochem.* **2025**, *29*, 3237–3251. [CrossRef]
56. Costentin, C.; Drouet, S.; Passard, G.; Robert, M.; Savéant, J.-M. Proton-coupled electron transfer cleavage of heavy-atom bonds in electrocatalytic processes. Cleavage of a C–O bond in the catalyzed electrochemical reduction of $CO_2$. *J. Am. Chem. Soc.* **2013**, *135*, 9023–9031. [CrossRef] [PubMed]
57. Azcarate, I.; Costentin, C.; Robert, M.; Savéant, J.-M. Through-space charge interaction substituent effects in molecular catalysis leading to the design of the most efficient catalyst of $CO_2$-to-Co electrochemical conversion. *J. Am. Chem. Soc.* **2016**, *138*, 16639–16644. [CrossRef] [PubMed]
58. Rebolledo, J.P.; Cruz-Ramírez, M.; Patakfalvi, R.; Tenorio-Rangel, F.J.; Ortiz-Frade, L.A. Insight on the mechanism of molecular catalysis of $CO_2$ reduction with Fe(II)-polypyridine complexes. *Electrochimica Acta* **2017**, *247*, 241–251. [CrossRef]
59. Berger, R.M.; Holcombe, J.R. An electrochemical and spectroelectrochemical investigation of bis(2,2′-bipyridine) (2,4,6-tris(2-pyridyl)triazine)ruthenium(II): A potential building block for supramolecular systems. *Inorganica Chim. Acta* **1995**, *232*, 217–221. [CrossRef]
60. Keszei, E. Kinetics of Composite Reactions. In *Reaction Kinetics*; Springer: Cham, Switzerland, 2021; pp. 71–116. [CrossRef]


**Disclaimer/Publisher's Note:** The statements, opinions and data contained in all publications are solely those of the individual author(s) and contributor(s) and not of MDPI and/or the editor(s). MDPI and/or the editor(s) disclaim responsibility for any injury to people or property resulting from any ideas, methods, instructions or products referred to in the content.